IET Generation, Transmission & Distribution

Research Article

IET Journals
The Institution of Engineering and Technology

Voltage sag influence on controlled three-phase grid-connected inverters according to the Spanish grid code

ISSN 1751-8687
Received on 4th October 2019
Revised 29th January 2020
Accepted on 3rd February 2020
E-First on 27th March 2020
doi: 10.1049/iet-gtd.2019.1496
www.ietdl.org

Mostafa Bakkar[1] ✉, *Santiago Bogarra*[1], *Alejandro Rolán*[2], *Felipe Córcoles*[1], *Jaume Saura*[1]

[1]*Department of Electrical Engineering, ETSEIAT-UPC, Colom St. 1, Terrassa, Barcelona, 08222, Spain*
[2]*Department of Industrial Engineering, IQS-URL, Via Augusta 390, Barcelona 08017, Spain*
✉ *E-mail: mostafa.bakkar@upc.edu*

Abstract: To ensure the safe operation of the grid, there are some requirements to be taken into consideration to connect power converters. During abnormal conditions – e.g. during voltage sags –, the control of the converters is a very important key to guarantee power quality and good behaviour of the distributed generation system. The aim of this study is to employ two possible control strategies for a grid-connected inverter according to the Spanish grid code, and to analyse the behaviour of the output voltages during both symmetrical and unsymmetrical voltage sags. The analytical development shows the sag influence on currents, voltages, active and reactive powers. These influences are explained through *Ku* transformation in the synchronous reference frame, thus giving a representation for electrical variables easiest to analyse. The results show how control strategies affect the converter behaviour and how they can support the main grid during faults through the control of active and reactive power injection. Sags with different durations and depths have been taken into account, which can provoke critical values for electrical magnitudes and can lead to the violation of the grid code. The proposed control strategies study has been validated by means of both simulations in MATLAB™–Simulink and experimental results.

Nomenclature

Variables

h	sag depth
i_{abc}	injected *abc* currents
I_{amax}	maximum active current
I_a, I_r	active and reactive currents
i_f	transformed injected current
i_{fREF}^{+}, i_{fREF}^{-}	forward Positive- and negative-reference currents
$\mathrm{Re}(i_f)$, $\mathrm{Im}(i_f)$	real and imaginary parts of the transformed injected current
$K(\Psi)$	*Ku* transformation
L, R	filter resistance and inductance
P_{a0}	supplied active power before sag
P_{REF}, Q_{REF}	reference active and reactive powers
p, q, s	instantaneous active, reactive and apparent powers
$V(t)$	instantaneous RMS remaining voltage
$v_a(t)$, $v_b(t)$, $v_c(t)$	instantaneous RMS voltages
$v_{abcpu}(t)$	per-unit *abc* voltages
v_{abcRef}	reference inverter *abc* voltages
V_{base}	voltage base value
V_{DC}	DC-link voltage
$v_{fpu}(t)$	per-unit transformed voltage
v_{fRef}	transformed reference voltage
v_{gabc}	grid *abc* voltages
v_{gf}	transformed grid voltage
v_{gf}^{+}, v_{gf}^{-}	grid voltage positive- and negative-sequence components
ΔV	symmetrical voltage range
Ψ	transformation angle
ω	grid pulsation

1 Introduction

Nowadays, there is a noticeable increase in smart grid research promoted by the growth of renewable energy penetration [1]. Grid faults may result in non-desired system disconnections due to overcurrent [2]. Therefore, one of the main aims of smart grids is to minimise the number of affected users during faults and to support the main grid [3].

Distributed generation (DG) systems connected to the main grid through converters have to be maintained in service during grid faults in order to balance generated and consumed powers [4, 5], so standards have to be developed in order to regulate the grid connection of renewable energy systems. It is reasonable to consider that the future distribution grid codes could be similar to those currently used in the transmission system. Consequently, during the voltage sag, the renewable energy generators should operate by increasing converter currents in order to achieve the grid code specifications [6].

According to grid codes, converters must remain connected to the grid during faults, reduce the active power injection and increase the reactive power injection in order to support the grid [7]. In DG systems, the control of power converters may have a strong influence on the grid behaviour. For this reason, it is important to propose analytical models that are useful to understand the response of grid-connected equipment under voltage sags. Motivated by this purpose, a detailed mathematical analysis of the currents during voltage sag is carried out in this paper in order to develop the proposed control scheme.

Most of faults in the grid are unbalanced faults, which deteriorate the performance of the grid-connected converters, thus negatively affecting the power quality of the grid. Unsymmetrical voltage sags (caused by unbalanced faults, i.e. one-phase-to-ground, two-phases or two-phases-to-ground faults), provoke grid current peaks and DC-bus voltage fluctuations, because due to the negative-sequence components, a pulsation of twice the fundamental frequency appear in both voltages and currents, causing a ripple in the injected power to the grid and in the DC-bus voltage [8]. Therefore, the negative-sequence currents need to be controlled, in order to inject more reactive power to the grid during faults to enhance the power quality standards of the grid. Hence, several studies have been published with the aim of controlling the reference current during unbalanced conditions in order to increase the injected reactive current [9–16]. In these references, the converter current control is done using *Park* transformation, while

in this paper *Ku* transformation is used to analyse the converter behaviour during sags in a simple way. By using the *Ku* transformation, it gives a clear visual representation of the electrical variables, and the most important information regarding sag depth and type can be more easily analysed than using *dq* representation, as will be discussed in Section 4. Next, the aforementioned references will be discussed.

In [9], a current control method is proposed to meet the low-voltage ride-through requirement, by controlling positive- and negative-sequence current components under unsymmetrical sags by means of an instantaneous grid voltage feedforward control; moreover, a fast voltage sag detection is proposed. A similar idea has been discussed in [10] based on controlling positive- and negative-sequence components of a large-scale grid-connected photovoltaic (PV) system under unbalanced voltage. That study has been done with the aim of delivering constant active power to the grid during voltage sags. Generalised power control strategies based on symmetrical components are proposed in [11], aiming to manage the delivered instantaneous power under unbalanced voltage sags. In [12, 13], different strategies for injecting reactive current during unbalanced grid faults have been studied. Mathematical expressions have been found to set the limit of the reactive power delivered by a static compensator during such transient unbalanced grid conditions. In [14], four different reactive power injection control strategies named average active reactive control, balanced positive-sequence control, instantaneous active reactive control and positive-negative-sequence control have been presented with different goals. The aim has been to study the active and reactive power delivered to the grid during unbalanced conditions, when different positive- and negative-sequence currents are injected. In [15], the same control strategies represented in [14] have been used in order to minimise the DC voltage oscillations and to achieve current limiting control. In order to satisfy the peak current limitation and maximum DC voltage oscillations criteria, a couple of reactive power reference values have been calculated for each control strategy. The delivered reactive power reference has been chosen by comparing reference values that will consider both DC voltage oscillation and peak current limitation.

Current limiting strategies are taken into account in order not to exceed the limits of the converter, but special attention should be taken not to obtain distorted injected current or to increase the duration of the transient periods. In [17], a current limiting strategy of inverter-based islanded microgrids (MGs) has been proposed to limit the magnitude of the current reference during faults, by applying a current limiting factor to the reference current. In [18], instantaneous saturation limit (ISL) and latched limit (LL) strategies with a variety of reset approaches are studied for inverter-interfaced DG, in order to test the system response during and after faults. The proposed limiting strategies need a long transient time to limit the faulted current that will provide distorted currents for many periods. In [19], a current control strategy is presented based on the two current limiting strategies proposed in [18] and in [20] the same limiting strategies are integrated with overcurrent and overload protection schemes. A comparison study between ISL and LL limiting strategies has been presented to demonstrate the merits and demerits of both strategies. In [21], a current limiter is developed, which can limit inverter currents at a pre-defined threshold during faults, which distorts the injected current in some cases due to crest clipping. In [22], a novel current limiting control strategy is proposed to achieve a flexible active and reactive power regulation. It can be observed that the strategy needs long duration to achieve to the steady state. It should be noted that the aforementioned studies have not considered neither the limit of the reference currents according to the grid code requirements nor the implementation of a control strategy according to such specifications, which has become very important nowadays due to the increase in the number of DG systems connected to the grid. In the present work, positive- and negative-sequence components of currents have been controlled according to the Spanish grid code using a different way to limit the current in order to support the grid without exceeding the converter limits and maintaining sinusoidal currents during the fault.

Several studies in the literature [16, 23–28] account for the application of grid codes for controlling converters based on Park transformation to calculate the reference currents using several proposals. For example, in [16] only symmetrical voltage sags have been taken into account to meet the Spanish grid code requirements for grid-connected PV power plants. The authors of [23–28] take into account both symmetrical and unsymmetrical voltage sags. In [23–25], oscillating active power and unbalanced currents are obtained. In [26], two different scenarios of power injection have been proposed. The first one aims to inject balanced currents, but both active and reactive powers oscillate, as stated in [28]. The second one aims to inject constant active power during sags. However, the reactive power oscillates and the injected current is unbalanced, as stated in [27].

The authors previous work [29] describes the injected current of a three-phase inverter with symmetrical and unsymmetrical voltage sags, using a mathematical model in *Ku* components. In the control strategy, it is assumed that the transformed inverter voltage remains constant in the synchronous reference frame at its prefault steady-state value. In the same way as [29], the present work studies the behaviour of a three-phase grid-connected inverter under symmetrical and unsymmetrical voltage sags. However, the present paper goes a step further because now two different control strategies are developed in order to accomplish with the Spanish grid code. These control strategies provide reference voltages calculated according to the reference currents obtained from grid code, so their values are different from the pre-faulted steady-state values. Another difference from [29] is that in the present study the converter limits are considered, and a methodology to limit the injected current during faults is presented.

As mentioned in the literature review, few papers studied the behaviour of the control strategies under grid codes during unsymmetrical sags [23–28]. Hence, in order to fill this gap, more research needs to be done in this area, especially for unsymmetrical voltage sags. Therefore, the objectives of this paper can be summarised as follows:

(i) Unlike [26–28], a new proposal is developed to calculate the reference currents in order to prioritise the reactive reference current; then, the active reference current is obtained in order to maximise its value without exceeding the converter limits.
(ii) A new current limiting strategy different from [17, 19] is proposed based on grid code requirements and converter limits.
(iii) Two proposed control strategies are studied according to the Spanish grid code, during symmetrical and unsymmetrical voltage sags:

(a) The first control strategy seeks to inject balanced currents during unsymmetrical sags.
(b) The second one aims to deliver constant instantaneous active power.
(iv) Unlike [16, 23–28], the *Ku* transformation has been used to calculate the reference currents and to achieve an obvious visual representation of the electrical parameters.

The proposed control strategy has been studied for DGs connected to a stiff grid. However, for a weak grid, a hierarchical droop-based control is required to act on the reactive and active power in order to control the voltage and frequency of the grid, respectively. The idea presented in [19] can be integrated with the proposed control strategy which is the future focus of the authors' research.

This paper is structured as follows. Firstly, an explanation about the Spanish grid code requirements is given. Secondly, two different strategies to calculate the reference current are described. Thirdly, an analytical model of a three-phase grid-connected inverter with an *RL* filter is carried out when subject to either symmetrical or unsymmetrical voltage sags. Fourthly, the sag parameters influence is analysed through the *Ku* transformation. Finally, the analytical study is validated through simulations in MATLAB™–Simulink and experimental results, right before the conclusion.

2 Spanish grid code requirements

Spanish governments have promoted a sort of legal frameworks regarding grid connection and technical requirements. In 2005, the Spanish government published a requirement, which was mainly focused on renewable energy sources [30]. In 2008, the draft version of response requirements to voltage sags from production facilities under the special regime (P.O.12.2) was launched [7], which contains the required active and reactive currents shown in Fig. 1. During sags, the inverter must be controlled according to the injected active current I_a and reactive current I_r. The instantaneous value of the RMS remaining voltage $V(t)$ is calculated according to the following equation [31]:

$$V(t) = \sqrt{\frac{v_a(t)^2 + v_b(t)^2 + v_c(t)^2}{3}}, \tag{1}$$

where $v_a(t)$, $v_b(t)$ and $v_c(t)$ are the instantaneous RMS values of the *abc* voltages.

The grid code does not provide a clear explanation on how to proceed when unsymmetrical faults occur. For this reason, in this paper a proposal on how to apply the grid code for both symmetrical and unsymmetrical faults is developed in Section 3. In order to explain how to proceed in case of unsymmetrical sags, an explanation is developed assuming a two-phase fault, which provokes type C sag according to [32]. The parameter h (assumed to be 0.3 for this explanation) corresponds to point III in Fig. 1 and it is related to the sag depth, which is defined according to Table 1 from [33]. From the phasor expressions given in that reference for type C sag, the per unit RMS values during the steady state of the fault assuming a sag depth $h = 0.3$ are calculating using

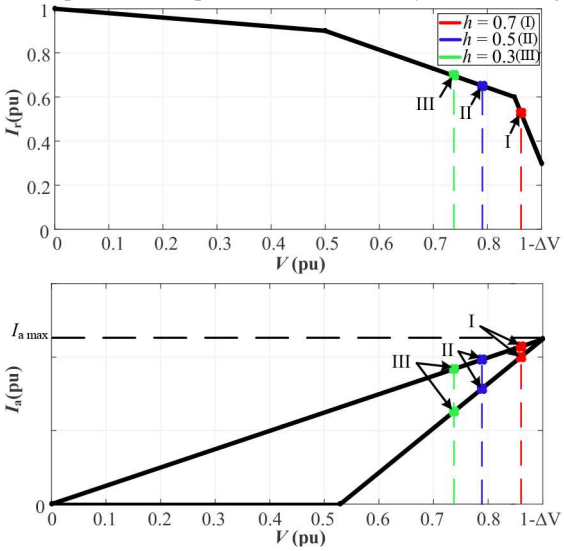

Fig. 1 *Active current (I_a) and reactive current (I_r) to be injected/absorbed during faults, according to Spanish grid code P.O. 12.2. h = sag depth. I, II and III points to be considered in this paper*

$$\begin{aligned} v_a(t) &= 1 \\ v_b(t) &= \sqrt{\left(-\frac{1}{2}\right)^2 + \left(-\frac{\sqrt{3}}{2}h\right)^2} = 0.5635 \\ v_c(t) &= \sqrt{\left(-\frac{1}{2}\right)^2 + \left(\frac{\sqrt{3}}{2}h\right)^2} = 0.5635. \end{aligned} \tag{2}$$

By substituting the values of (2) in (1), we obtain $V(t) = 0.739$ pu. According to this voltage and using Fig. 1, the active I_a and reactive I_r currents can be obtained, assuming that these values correspond to the positive sequence. The maximum active current $I_{a\,max}$ depends on the maximum values of the converter power before the sag.

For renewable energy resources, the value of $I_{a\,max}$ depends on the weather conditions, and its value can be obtained by means of the following equation [7]:

$$I_{amax} = \frac{P_{a0}}{1 - \Delta V}, \tag{3}$$

where ΔV is the symmetrical voltage range around the rated voltage (which equals 7.5% in distribution grids [7]), and P_{a0} is the active power supplied by the installation before the sag.

Once the values of active and reactive currents (I_a and I_r) are determined from the grid code, the converter limits need to be verified in order not to exceed the rated current

$$\sqrt{I_r^2 + I_a^2} \leq 1\,\text{pu}\,. \tag{4}$$

If the current obtained from (4) exceeds the rated current of the converter, then more priority is suggested to be given to the reactive power to give more support to the grid (this is one of the main differences from the references analysed in Section 1), as shown in the following equation:

$$I_a = \sqrt{1 - I_r^2}\,. \tag{5}$$

Table 1 Equations for reference active and reactive power, and negative-sequence current of control methods mentioned in Section 3.2, according to the Spanish grid code

Control method	Positive-sequence component	Negative-sequence component	Reference active and reactive powers
CPC	$i^+_{fREF} = \frac{1}{\sqrt{2}}(I_a + jI_r)$	$i^-_{fREF} = \frac{1}{2}\left(\begin{matrix}\mathrm{Re}\{i^+_{fREF}\}\left(\frac{-\mathrm{Re}\{v^+_{gf}\}\mathrm{Re}\{v^-_{gf}\} + \mathrm{Im}\{v^+_{gf}\}\mathrm{Im}\{v^-_{gf}\}}{\lvert v^+_{gf}\rvert^2}\right) \\ +\mathrm{Im}\{i^+_{fREF}\}\left(\frac{-\mathrm{Re}\{v^+_{gf}\}\mathrm{Im}\{v^-_{gf}\} - \mathrm{Im}\{v^+_{gf}\}\mathrm{Re}\{v^-_{gf}\}}{\lvert v^+_{gf}\rvert^2}\right)\end{matrix}\right) + j\left(\begin{matrix}\mathrm{Re}\{i^+_{fREF}\}\left(\frac{-\mathrm{Re}\{v^+_{gf}\}\mathrm{Im}\{v^-_{gf}\} - \mathrm{Im}\{v^+_{gf}\}\mathrm{Re}\{v^-_{gf}\}}{\lvert v^+_{gf}\rvert^2}\right) \\ +\mathrm{Im}\{i^+_{fREF}\}\left(\frac{-\mathrm{Re}\{v^+_{gf}\}\mathrm{Re}\{v^-_{gf}\} - \mathrm{Im}\{v^+_{gf}\}\mathrm{Im}\{v^-_{gf}\}}{\lvert v^+_{gf}\rvert^2}\right)\end{matrix}\right)$	$P_{REF} = \frac{\lvert v^+_{gf}\rvert^2 - \lvert v^-_{gf}\rvert^2}{2\cdot\lvert v^+_{gf}\rvert^2}\left(\begin{matrix}\mathrm{Re}\{v^+_{gf}\}\mathrm{Re}\{i^+_{fREF}\} \\ +\mathrm{Im}\{v^+_{gf}\}\mathrm{Im}\{i^+_{fREF}\}\end{matrix}\right)$ $Q_{REF} = \frac{\lvert v^+_{gf}\rvert^2 + \lvert v^-_{gf}\rvert^2}{2\cdot\lvert v^+_{gf}\rvert^2}\left(\begin{matrix}\mathrm{Im}\{v^+_{gf}\}\mathrm{Re}\{i^+_{fREF}\} \\ -\mathrm{Re}\{v^+_{gf}\}\mathrm{Im}\{i^+_{fREF}\}\end{matrix}\right)$
BCC	$i^+_{fREF} = \frac{1}{\sqrt{2}}(I_a + jI_r)$	$i^-_{fREF} = 0$	$P_{REF} = \frac{1}{2}\left(\begin{matrix}\mathrm{Re}\{v^+_{gf}\}\mathrm{Re}\{i^+_{fREF}\} \\ +\mathrm{Im}\{v^+_{gf}\}\mathrm{Im}\{i^+_{fREF}\}\end{matrix}\right)$ $Q_{REF} = \frac{1}{2}\left(\begin{matrix}\mathrm{Im}\{v^+_{gf}\}\mathrm{Re}\{i^+_{fREF}\} \\ -\mathrm{Re}\{v^+_{gf}\}\mathrm{Im}\{i^+_{fREF}\}\end{matrix}\right)$

CPC, constant active power control; BCC, balanced current control.

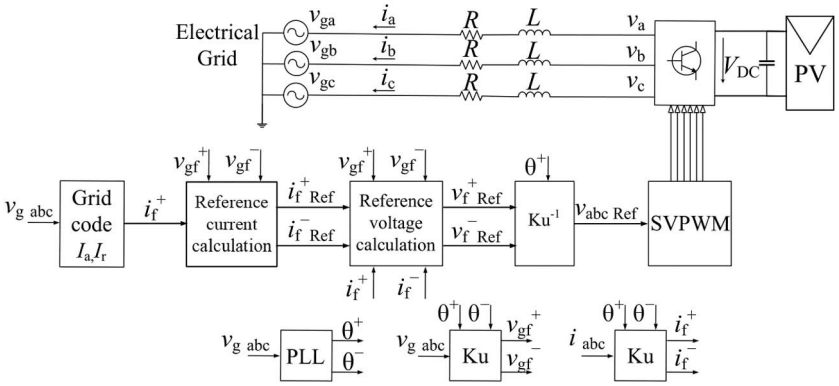

Fig. 2 *General scheme of a three-phase grid connected inverter supplied by PV and its control*

3 Theoretical analysis of a three-phase grid-connected inverter under voltage sags according to the Spanish grid code

3.1 Analytical model in Ku variables

This section explains the mathematical model of the converter using *Ku* transformation. Fig. 2 shows the general scheme of a three-phase inverter connected to a grid. A PV generator delivers power to the DC side of an inverter, which converts it into AC power by means of controlling the injected active and reactive currents, according to the grid code.

The mathematical expressions of the *abc* variables that model the system of Fig. 2 (considering the generator-sign convention) are given in the following equation:

$$\begin{bmatrix} v_{a\mathrm{Ref}} \\ v_{b\mathrm{Ref}} \\ v_{c\mathrm{Ref}} \end{bmatrix} = \begin{bmatrix} R & 0 & 0 \\ 0 & R & 0 \\ 0 & 0 & R \end{bmatrix} \begin{bmatrix} i_a \\ i_b \\ i_c \end{bmatrix} + \frac{\mathrm{d}}{\mathrm{d}t} \begin{bmatrix} L & 0 & 0 \\ 0 & L & 0 \\ 0 & 0 & L \end{bmatrix} \begin{bmatrix} i_a \\ i_b \\ i_c \end{bmatrix} + \begin{bmatrix} v_{ga} \\ v_{gb} \\ v_{gc} \end{bmatrix}, \tag{6}$$

where $v_{abc\ \mathrm{Ref}}$ are the *abc* components of the reference voltage of the inverter, $v_{g\ abc}$ are the *abc* components of the grid voltage, i_{abc} are the injected *abc* currents from the inverter to the grid and R and L are the resistance and the inductance of the filter, respectively.

The mathematical study is developed using the complex form of the *Park* transformation, i.e. *Ku* transformation, which gives an easiest representation can be used to analyse the electrical variables. The power-invariant form of the *Ku* transformation is given by [34]

$$[\boldsymbol{K}(\Psi)] = \frac{1}{\sqrt{3}} \begin{bmatrix} 1 & e^{\mathrm{j}\Psi} & e^{-\mathrm{j}\Psi} \\ 1 & a^2 e^{\mathrm{j}\Psi} & a e^{-\mathrm{j}\Psi} \\ 1 & a e^{\mathrm{j}\Psi} & a^2 e^{-\mathrm{j}\Psi} \end{bmatrix}; \quad a = e^{\mathrm{j}2\pi/3}$$
$$[x_{abc}] = [\boldsymbol{K}(\Psi)][x_{0\mathrm{fb}}] \quad ; \quad [x_{0\mathrm{fb}}] = [\boldsymbol{K}(\Psi)]^{-1}[x_{abc}], \tag{7}$$

where the subscripts a, b and c stand for the *abc* components of the variable x (voltage or current). The subscripts 0, f and b stand for the *zero*, *forward* and *backward* components, respectively, and Ψ is the transformation angle provided by a PLL assuming the synchronous reference frame. *Backward* components are the complex conjugate of *forward* components, so only *forward* components need to be used. By applying the *Ku* transformation (7) into (6), and assuming the sag in its steady-state condition with sinusoidal waves, we obtain

$$v_{\mathrm{fRef}} = [R + L(s + \mathrm{j}\omega)]i_{\mathrm{f}} + v_{\mathrm{gf}}, \tag{8}$$

where $v_{\mathrm{f\,Ref}}$ is the transformed inverter reference voltage, $s = \mathrm{d}/\mathrm{d}t$ is the derivative operator, i_{f} is the transformed injected current and v_{gf} is the transformed grid voltage. Under unbalanced conditions, transformed grid voltage can be represented by using the *Fortescue* transformation [35] as

$$v_{\mathrm{gf}}^+ = \frac{1}{\sqrt{6}}\left(V_a e^{\mathrm{j}\varphi_{V_a}} + aV_b e^{\mathrm{j}\varphi_{V_b}} + a^2 V_c e^{\mathrm{j}\varphi_{V_c}}\right) \tag{9}$$

$$v_{\mathrm{gf}}^- = \frac{1}{\sqrt{6}}\left(V_a e^{-\mathrm{j}\varphi_{V_a}} + aV_b e^{-\mathrm{j}\varphi_{V_b}} + a^2 V_c e^{-\mathrm{j}\varphi_{V_c}}\right) \tag{10}$$

$$v_{\mathrm{gf}} = v_{\mathrm{gf}}^+ + v_{\mathrm{gf}}^- e^{-\mathrm{j}2\omega t}. \tag{11}$$

The same procedure can be followed to obtain the transformed injected current from the inverter to the grid, so

$$i_{\mathrm{f}} = i_{\mathrm{f}}^+ + i_{\mathrm{f}}^- e^{-\mathrm{j}2\omega t}. \tag{12}$$

3.2 Proposed control techniques under the Spanish grid code requirements

The power injected into the grid is affected by the positive and negative-sequence components of the injected currents during the sag [13]. Therefore, if the negative sequence of the grid current is not controlled, the injected power will oscillate at twice the grid frequency. This control must have the ability to ride through any kind of faults, by increasing the injection of reactive power into the grid, and reducing the active power injection during the fault [11]. For symmetrical sags, the negative-sequence component of the current is not considered (in other words, it is assumed to be zero), but for unsymmetrical sags this component needs to be controlled. The aim of this paper is to obtain both positive and negative components using the *Ku* transformation according to the Spanish grid code. It should be noted that the proposed control strategies can be adapted to grid codes from other countries; the main differences between them lie in Fig. 1, because different grid codes may lead to a different amount of active and reactive currents to be injected during the sag [36]. As a result, depending on the sag depth, the values of I_{a} and I_{r} shown in Fig. 1 may be different for grid codes from other countries.

According to the instantaneous power theory developed in [37], positive- and negative-sequence reference values of transformed currents according to *Park* transformation are calculated. Based on this approach, different control algorithms under unsymmetrical sags for three-phase inverters have been implemented [14]. Note that the aim of this work is based on using *Ku* transformation to analyse the grid behaviour during sags, depending on different control strategies. Two different control strategies are proposed:

- Balanced current control (BCC) strategy: the aim is to inject balanced currents into the grid, but active and reactive powers will oscillate. In order to achieve that goal, this strategy imposes zero negative-sequence current.
- Constant active power control (CPC) strategy: it seeks to inject more reactive power, while keeping the injection of constant active power into the grid, but the injected currents are unbalanced. To obtain that goal, this strategy controls the negative-sequence component of the current.

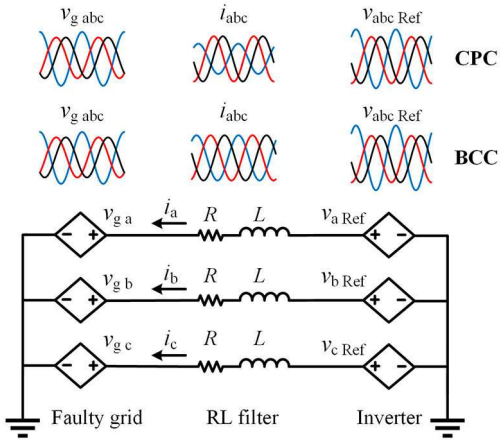

Fig. 3 *Equivalent circuit for a three-phase inverter with RL filter under a faulty grid controlled by the proposed CPC and BCC strategies*

The change in value in the negative-sequence component will cause a variation in the reference active and reactive power calculation, as shown in Table 1. Fig. 3 shows the equivalent circuit that corresponds to (6), where the *abc* components of the inverter are given by their reference value.

Moreover, a visual example of how a two-phase fault affects the behaviour of the electrical variables is shown in that figure with the two control strategies considered in this paper. The reference currents are going to be evaluated according to Spanish grid code discussed in Section 2. The control system of the three-phase inverter is shown at the bottom of Fig. 2 to calculate the reference currents. Given the lectures of the grid voltages ($v_{g\,abc}$) at the point of common connection, both active and reactive currents (I_a and I_r) are obtained according to (1) and Fig. 1. The reference positive-transformed currents are imposed directly from grid code by using

$$i_{f\,REF}^{+} = \frac{1}{\sqrt{2}}(I_a + jI_r), \tag{13}$$

where subscript f stands for the *forward* component of the transformed *Ku* variable. Note that the active current I_a corresponds to the real part of the positive-transformed forward reference current, while the reactive power I_r matches the imaginary part. Using the positive reference currents, the reference values for the active and reactive powers (P_{REF} and Q_{REF}) are calculated for each control technique according to Table 1.

The calculation of the negative reference currents can be obtained in two different ways. The first one is by imposing zero negative reference currents (BCC strategy), and the second one is by calculating the negative reference currents using the equations of the middle column of Table 1 (CPC strategy). When imposing zero negative currents, there will be no oscillation in i_f; otherwise, i_f will oscillate. During the faults, I_a and I_r currents are updated in order to match with the grid code, so the active and reactive powers will vary. Fig. 4 shows the behaviour of each control strategy during a two-phase fault (type C sag) with different depths of $h =$ 0.7, 0.5 and 0.3, whose *abc* voltage components are shown in the first row. Assuming that the converter injects 70% of its rated power before the fault, then $P_{a0} = 0.7$ in (3). The second row of Fig. 4 shows that currents are unbalanced when applying CPC strategy, while they are balanced when applying BCC strategy during unsymmetrical sags; in both cases, the injected currents are limited to the rated current of the converter. The third and fourth rows of Fig. 4 show the real and imaginary parts of the transformed forward component of the reference current. It is observed that there is an oscillation in that current for CPC strategy, which means in some cases this strategy will not be able to validate the grid code for unsymmetrical sags, while for BCC strategy this current remains constant, which means that the grid code have been validated.

The limits that appear in the third and fourth rows of Fig. 4, named as I, II and III, correspond to the grid code limits for active and reactive currents shown in Fig. 1. If the imposed *abc* current does not exceed 1 pu, the control imposes the upper limit for the active current, i.e. real part of the positive component of the injected current, according to (13). Nevertheless, if that current exceeds 1 pu, the control must decrease the injected active current until its value is between the limits shown in Fig. 1. While for the reactive current, i.e. imaginary part of the positive component of the injected current, as shown in (13), there is only one possible value, according to Fig. 1. For example, in the second row of Fig. 4*a*, the control imposes the upper limit of the active current for the sag with depth $h = 0.7$, assuring that the *abc* current does not exceed 1 pu. However, in Fig. 4*b* for $h = 0.5$, if the upper limit of the active current is injected, the *abc* current exceeds 1 pu, so a limitation must be introduced in this case in order to always inject *abc* current within 1 pu (solid black line in the third row of Fig. 4). In some cases, even if the control injects the lower limit of the active current, the injected *abc* current will exceed 1 pu, as shown in the second row of Fig. 4*c*. It is observed from the third and fourth row of Fig. 4 that CPC strategy cannot always achieve the grid code, because the injected currents go beyond the aforementioned limits, while for the BCC strategy the limits are not exceeded.

It is observed that for CPC strategy the negative sequence of the injected current has a value different from zero, while for the BCC strategy this value is zero. With respect to that point, the authors previous work [38] has also shown that BCC strategy is the only one that can validate the grid code without limitations for unsymmetrical sags. For symmetrical sags both control will be able to verify the grid code, because in this case, the negative sequence component will be zero. However, this strategy has the drawback that there is an oscillation in the instantaneous active power (p), as seen in the fifth row of Fig. 4, while for the CPC strategy there is no oscillation in that power. Regarding the instantaneous reactive power (q), the sixth row of Fig. 4 shows that there is an oscillation in it, but with CPC strategy, the oscillation in that power is bigger. The seventh row of Fig. 4 shows that there is an oscillation for the instantaneous apparent power (obtained from (14)) in both control strategies, and this oscillation cannot be eliminated because either active or reactive powers have an oscillation

$$s = \sqrt{p^2 + q^2}\,. \tag{14}$$

The last row of Fig. 4 represents the active–reactive (p–q) curve. It is observed that for CPC strategy this curve is represented by a straight line because there is no oscillation in the active power. However, for BCC strategy both powers will oscillate, so the straight line transformed into a circle.

3.3 Flowchart

To sum up the theoretical analysis, the procedure to be followed in order to adapt the Spanish grid code into the control system is described below. Fig. 5 shows the flowchart for that purpose.

Firstly, the per unit instantaneous value of the RMS remaining voltage during the sag is obtained according to (1). Secondly, by means of the previous value, the active and reactive currents are obtained according to the Spanish grid code, which is depicted in Fig. 1; next, the upper limit of the active current is selected. Thirdly, these currents are used to obtain the *Ku* transformed positive reference current according to Table 1. With respect to the *Ku* transformed negative reference current, it is calculated by means of Table 1 depending on the adopted control strategy. Fourthly, the *Ku* transformed components of the grid voltage and injected currents are obtained by means of (11) and (12), respectively (note that in order to obtain the transformed grid voltage, (9) and (10) have to be used). Finally, the mathematical model of the whole system is obtained by using (8). Finally, the *abc* components of the reference voltage for the inverter are calculated by using (7) as

$$[v_{abc\,Ref}] = [\boldsymbol{K}(\Psi)][v_{f\,Ref}]\,. \tag{15}$$

The *abc* currents are calculated to ensure that the value does not exceed 1 pu. If the value exceeded that limit, the active current would need to be reduced within the limits of the grid code as shown in Fig. 1, until the *abc* current equals 1 pu.

It should be noted that, the proposed analytical model describes the behaviour of a three-phase grid-connected inverter with *RL* filter under unsymmetrical voltage sags. Note that this model is also valid for symmetrical sags. In this case, the negative-sequence component of the grid voltage is zero, i.e. $v_{gf}^{-} = 0$.

4 Analysis of sag parameters influence using *Ku* transformation

Different types of fault can be easily identified if voltages are represented in the complex plane, i.e. *Ku* plane, which will lead to

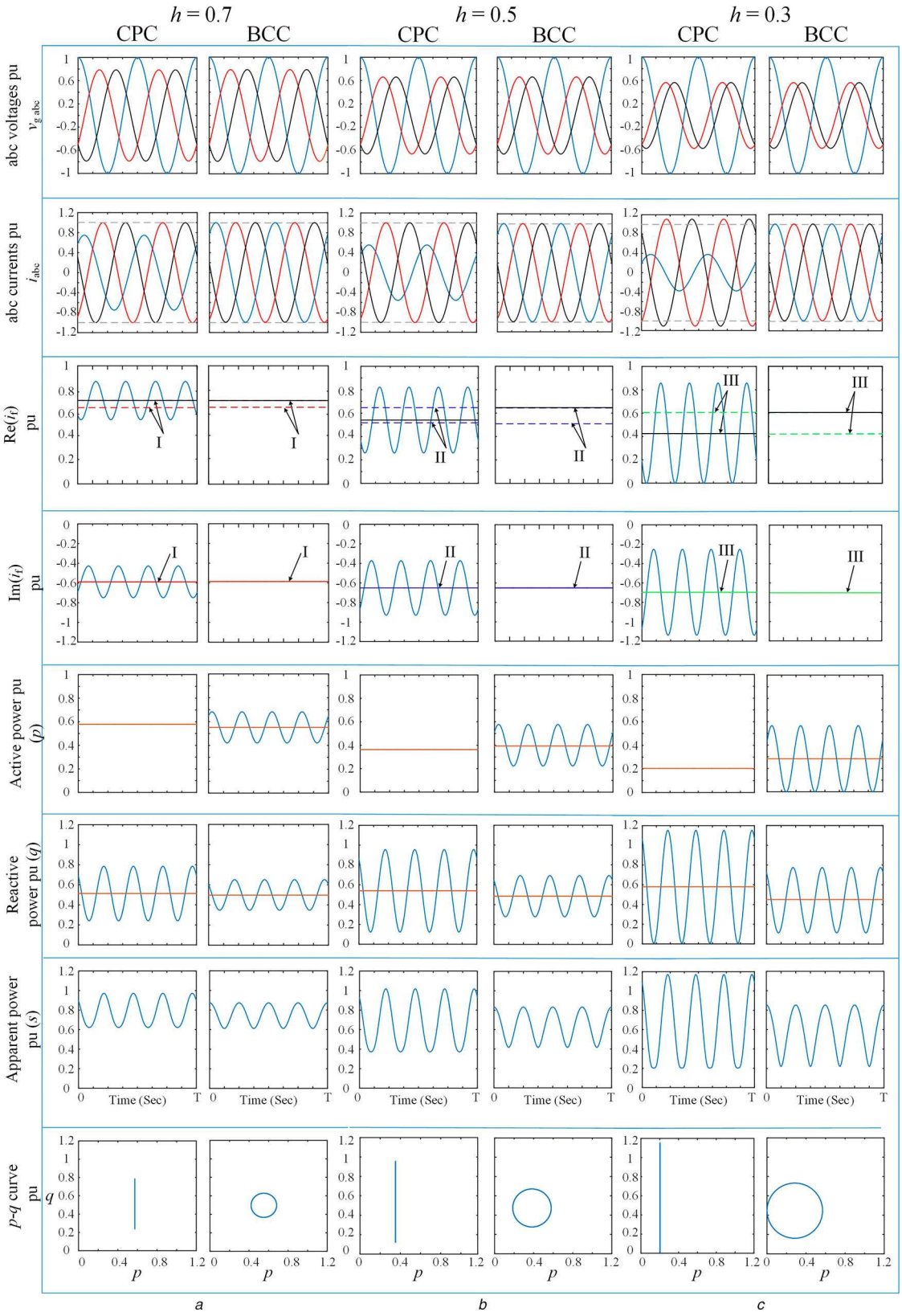

Fig. 4 *CPC and BCC strategies during a two-phase fault (type C sag) for sag depth*
(a) $h = 0.7$, ***(b)*** $h = 0.5$, ***(c)*** $h = 0.3$

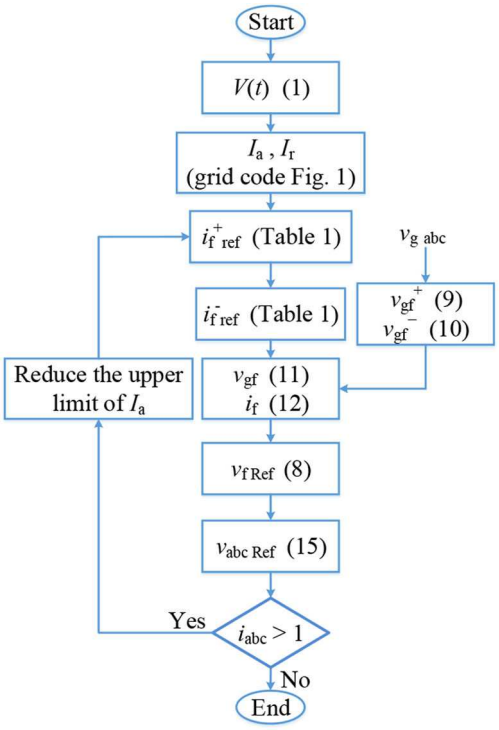

Fig. 5 *Flowchart to be followed to adapt the Spanish grid code to the electrical system of a grid-connected inverter*

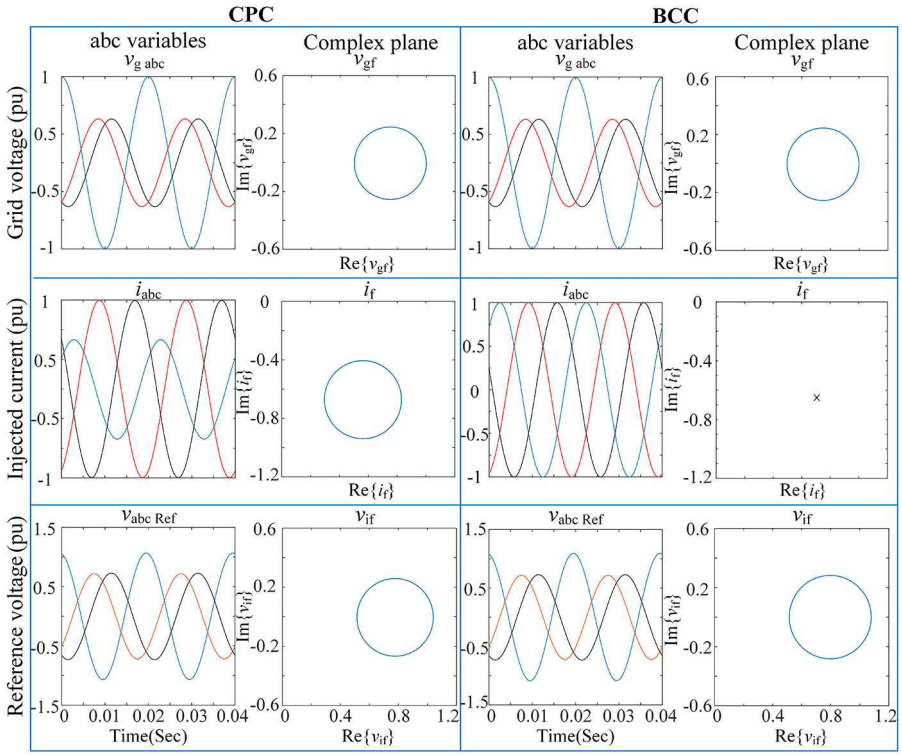

Fig. 6 *abc and complex plane of grid voltage, injected current and inverter reference voltage with h = 0.5 sag depth for unsymmetrical sag (type C)*

a simpler way to know and recognise the sag type and depth. In this section, the *abc* and transformed voltages are represented in per unit values, according to

$$v_{fpu}(t) = v_f(t)/(\sqrt{3/2}V_{base})$$
$$v_{abcpu}(t) = v_{abc}(t)/(\sqrt{2}V_{base}), \quad (16)$$

where V_{base} is the voltage base value, which corresponds to the phase voltage.

Fig. 6 shows the time evolution of the waveform in *abc* and transformed variables of the grid voltage, injected current and reference inverter voltage during unsymmetrical sags (type C sag). It is observed that due to the unbalance between the phases, the transformed variables of the grid voltage and reference inverter voltage have an oscillation, which is observed by the circle waveform in the complex plane. However, the BCC strategy always imposes symmetrical current, so there is no oscillation in the transformed current (note that there is a single point, but not a circle in the complex plane of the current). Moreover, note that in the CPC strategy the current is unbalanced during the sag, so an oscillation will appear in this case, as shown by the circle. This is explained by the exponential term that depends on twice the fundamental pulsation, $e^{-j2\omega t}$, which appears in (12). For

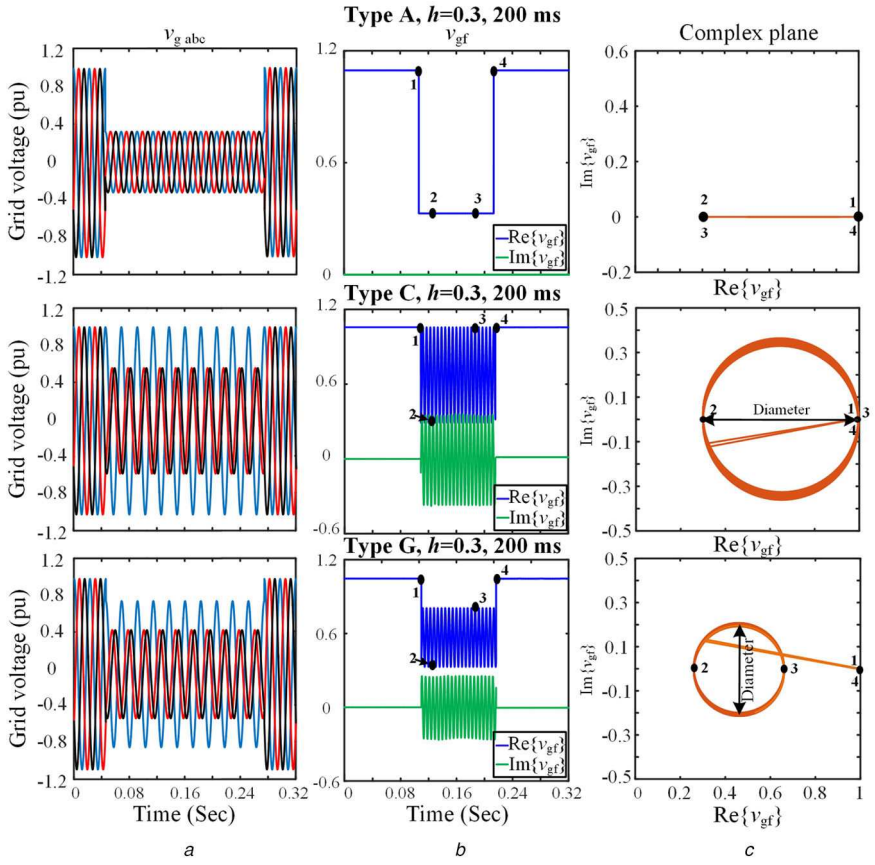

Fig. 7 *Differences between type A, type C and type G sags using transformed variables with h = 0.7 sag depth, and 200 ms duration*
(a) *abc* variables, ***(b)*** Transformed variables, ***(c)*** Complex plane

symmetrical sags (type A sag), it is observed that CPC and BCC strategies give the same time evolution in *abc* and complex plane (imaginary part versus real part). Because during the sag, all three phases of the grid voltage are balanced, which means there is no oscillation in the transformed variables of the voltage or the current, which will be represented as a single point in the complex plane.

Fig. 7 shows the time evolution of both *abc* components and transformed components of the grid voltage before, during and after a fault, considering: symmetrical sags (or type A sags, which are caused by three-phase faults) and unsymmetrical sags type C (which is caused by phase-to-phase faults) and type G (which is caused by phase-to-phase-to-ground faults after two Dy transformers). In this figure, point 1 represents the starting point of the sag, while points 2 and 3 represent the minimum and maximum oscillation of the sag, respectively, and point 4 represents the end of the sag. Note that in Fig. 7*b* for type A sag, points 2 and 3 are in the same position in Fig. 7*c*, because there is no oscillation in the representation of the real and imaginary parts. For this reason, the complex plane of the voltages gives a straight line, which means that the fault is symmetrical. However, for type C sag points 1, 3 and 4 are in the same level, as shown in Fig. 7*b*, because only two phases have a reduction in voltage. Due to this fact, the representation in the complex plane is not a straight line (as in the case of symmetrical sags), but a circle. However, it should be noted that this representation is not the same for different unsymmetrical sag types. Indeed, Fig. 7*b* shows for type G sag that points 1, 3 and 4 are not in the same level as in the case of type C sag. This is due to the fact that the voltage is reduced in all phases, as shown in Fig. 7*a* for type G sag. As a result, it is observed from Fig. 7*c* that the circle moves to the left in this case, because there is a voltage reduction in all the phases. As shown in Fig. 7, for the same sag type and using the complex plane, the sag depth affects the length of diameter. The diameter of the circle in the complex plane for unsymmetrical sag can be used to identify the unbalance between the phases. For example, note that the unbalance between phases for type C sag is higher than for type G sag. That is why the diameter of the circle is higher for type C than for type G. Another advantage of using the complex plane, i.e. *Ku* plane to represent the grid voltages is that it gives information about the location of the end point of the sag (point-on-wave). For example, looking at Fig. 8 the following conclusions are drawn: when the sag duration is a multiple of a period, then the starting point (point 1) and the ending point (point 2) of the sag are located at the same place in the complex plane (Fig. 8*c*), while if the sag duration is not a multiple of a period, then points 1 and 2 are located in different places for unsymmetrical sags. Indeed, note that for unsymmetrical sag type C when the sag duration is 200 ms (multiple of a period), both points 1 and 2 are placed at the rightmost part of the circle (Fig. 8*c*). However, if the sag duration is 225 ms (not a multiple of a period), then points 1 and 2 are in different places because the point-on-wave where the sag finishes is different for various durations. Otherwise, for symmetrical sags (type A sag), points 1 and 2 are always located in the same place, because the point-on-wave when the sag ends will always be the same. To sum up, the location of the end point of the sag will be always the same in the complex plane for symmetrical sags, but for unsymmetrical sags, it is a useful tool to visualise the exact end point of the sag. The previous results show that visualising grid voltages in the complex plane gives better visual representation of the sag parameters influence.

5 Experimental results and discussion

The experimental setup shown in Fig. 9*a* is used to validate the analytical model and the simulation results in MATLAB™–Simulink.

Table 2 shows the system parameters. The system consists of a smart three-phase AC power source to emulate the grid and a converter connected to the grid through an *RL* filter. Fig. 9*b* depicts the electrical scheme of the experimental setup. In order to implement the control algorithms using MATLAB™ software and ControlDesk, grid voltages ($v_{g\ abc}$), line currents (i_{abc}) and DC-link voltage (V_{DC}) need to be measured by means of measuring devices,

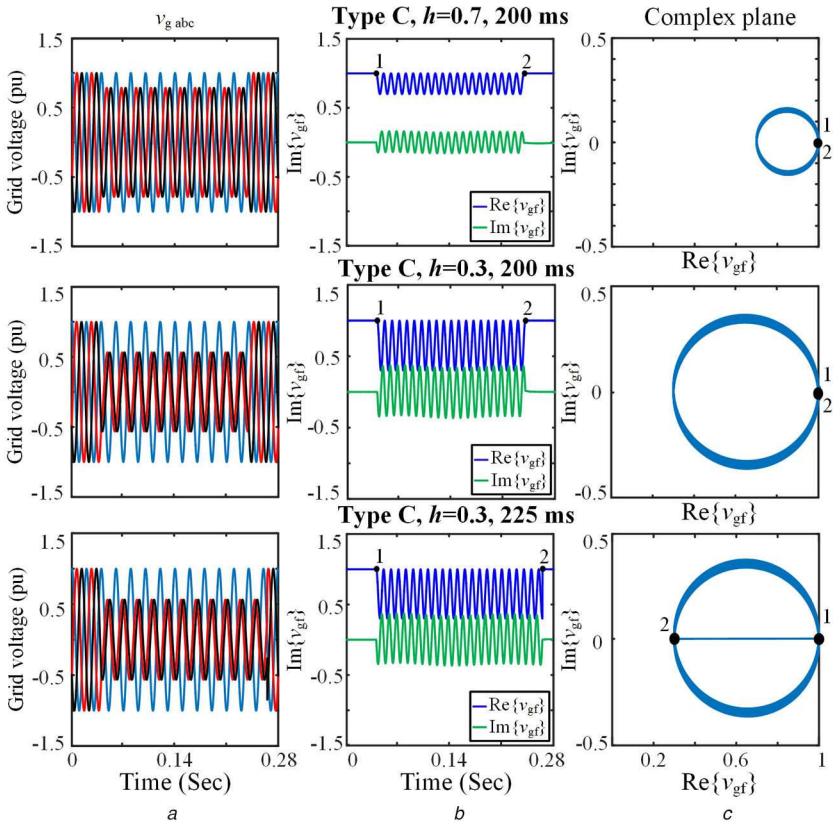

Fig. 8 *Influence of sag depth and sag duration*
(a) *abc* variables, ***(b)*** Transformed variables, ***(c)*** Complex plane

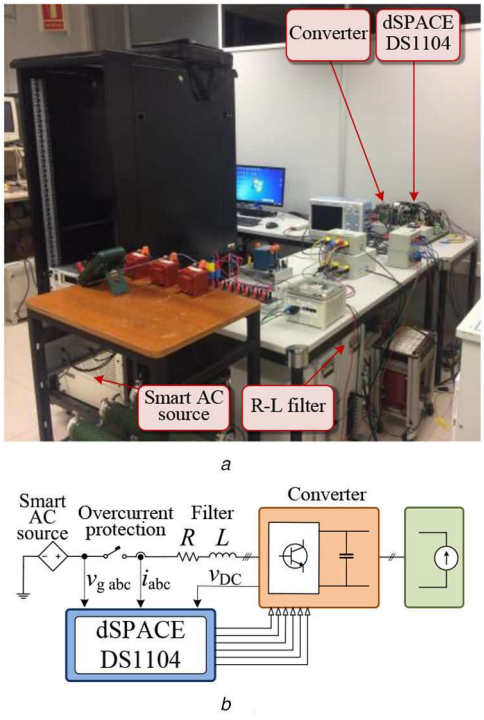

Fig. 9 *Experimental setup*
(a) Real setup, ***(b)*** Electrical scheme

Table 2 System parameters

inverter	rated power	10 kVA
	rated voltage	400 V
filter	inductance (L)	10 mH
	resistance (R)	0.2 Ω
DC bus	DC rated voltage	800 V

which are sent to an oscilloscope and to the dSPACE™ DS1104, which is connected to a PC.

A voltage sag with depth $h = 0.5$ was applied when the system was operating in steady-state conditions. As shown in Fig. 10, the control strategies presented in Section 3 have been validated for symmetrical and unsymmetrical sags, in order to show their ability to validate the Spanish grid code requirements. The obtained results show that for symmetrical sags both strategies inject the upper limit of the active current, because in this case, the negative-sequence voltage is zero, so the injected current is balanced. Nevertheless, for unsymmetrical sags, it is observed that the injected currents do not exceed the grid code limits for BCC strategy when the upper limit of the active current is injected. Moreover, it injects symmetrical current, because this strategy imposes zero value for the negative reference current. But for CPC strategy, if the upper limit of the active power is injected, the current exceeds these limits (point II at Fig. 1), so in this case a reduction in the active current must be calculated in order not to exceed 1 pu according to (5) (solid black line in Fig. 10 for type C sag with CPC). In addition, for CPC the injected current is unbalanced, because the negative-sequence currents have a value different from zero.

In the proposed strategies, the current control loop provides an advantage to restrict the currents to limited values, which will prevent overloading conditions at steady state during the fault. However, for transient condition (at the start and at the end of the sag) the current signal does not exceed 1.5 pu in all the analysed cases for different sag types with different depths, as seen in Fig. 10.

Fig. 11 shows the theoretical, simulated and experimental grid voltage and injected current during unsymmetrical sags (type C) with depth $h = 0.5$. Both control strategies are tested under the same conditions. It is observed that when the voltage sag originates, both strategies inject the rated current of the converter in order to validate the grid code requirements. In case of symmetrical sags, the complex plane for both strategies will be a point, because the voltage and the current during the sag is balanced. As shown in that figure, CPC strategy injects unbalanced currents into the grid, so the transformed variables (real and

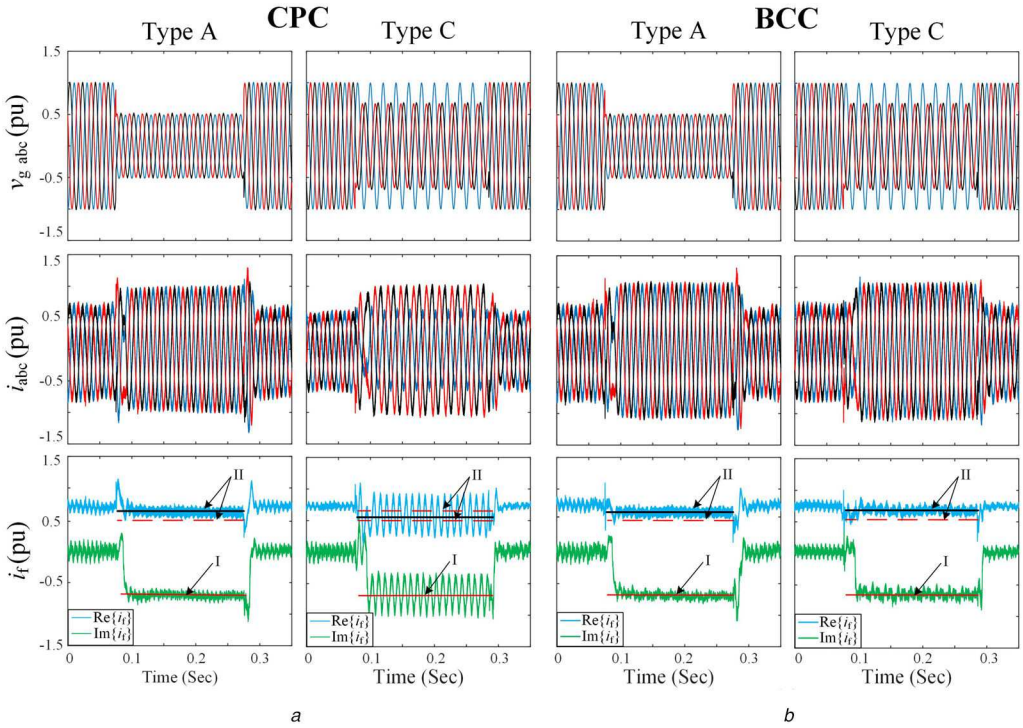

Fig. 10 *Experimental results of grid voltage and injected current with sag of h = 0.5 depth and 200 ms duration for*
(a) CPC strategy, ***(b)*** BCC strategy. I and II are the reactive and active current references, respectively, imposed by the Spanish grid code for a sag depth of $h = 0.5$ (Fig. 1)

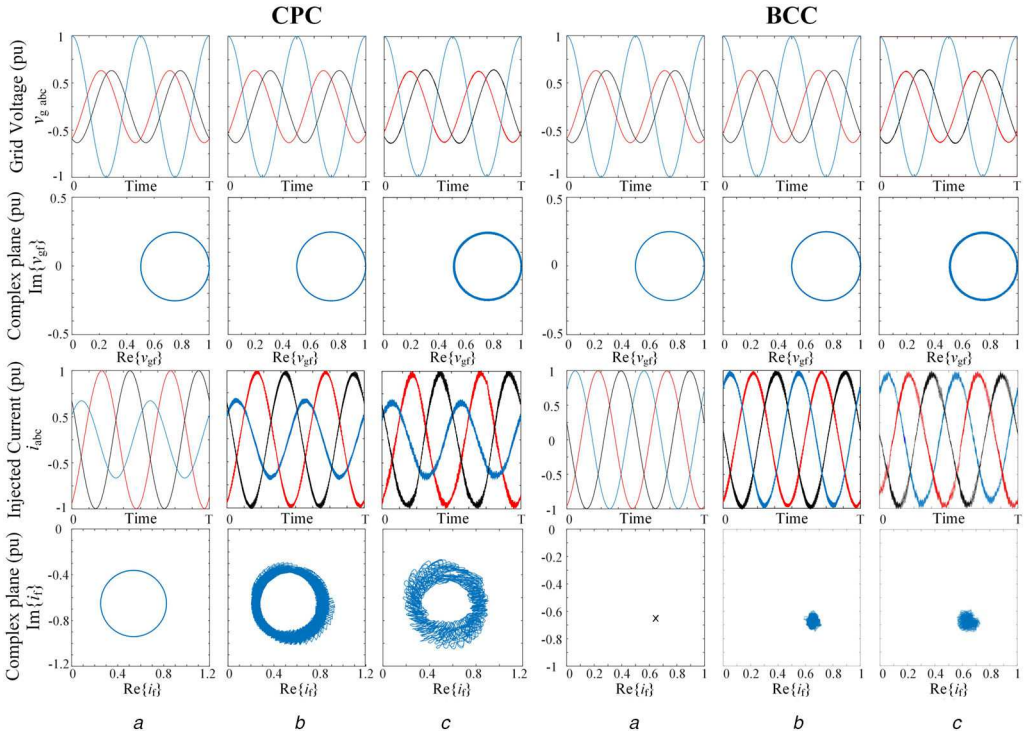

Fig. 11 *Results compare of CPC and BCC control strategies during unsymmetrical sag (type C)*
(a) Theoretical, ***(b)*** Simulation, ***(c)*** Experimental results, where T = period

imaginary) of the injected current are oscillating, which produces a circle, as shown in the complex plane. However, BCC strategy injects balanced currents during sags, so their representation in the complex plane corresponds to a point. It should be noted that in the theoretical results the representation is either a pure circle (for CPC strategy) or a point (BCC strategy), and for simulation results the representation has some noise due to the real model of the converter and its commutation frequency. The same is true for experimental results, but with more noise due to real system implementation. However, it can be concluded that theoretical, simulation and experimental results agree.

6 Conclusion

This study has proposed two different control strategies for a grid-connected inverter under voltage sags according to the Spanish grid code, named CPC and BCC strategies.

An analytical study has been presented by using the *Ku* transformation (i.e. complex form of *Park* variables), in order to represent the sag influence on the converter voltage and injected current in an easy way, as well as on the injected active and reactive powers.

The control strategies have been validated analytically, by simulation and by laboratory experiments for DGs connected to a

stiff grid, considering symmetrical and unsymmetrical sags with different durations and depths. The influence of these sag parameters has also been visualised in the complex plane. The proposed control and limiting strategies have been studied for DG connected to a stiff grid, however for a weak grid or a MG, another study need to be done in order to validate the proposed control for these types of grids, which is the authors' future research.

The results have shown that neither CPC or BCC strategies violate the grid code for symmetrical sags. Regarding unsymmetrical sags, only the BCC strategy always meets grid code requirements at the expense of oscillations in instantaneous active and reactive powers. In contrast, CPC strategy allows obtaining constant active power but it does not meet grid code requirements under unsymmetrical sags because transformed current oscillations are always outside the grid code limits. Fortunately, the average transformed current is outside the code limits only under the most severe unsymmetrical sags. Therefore, the authors suggest that the future grid code versions should specify how to proceed under unsymmetrical sag conditions. For example, grid codes could specify if they allow having unbalanced injected currents or an oscillation in the instantaneous active or reactive powers.

7 References

[1] Luo, Y., He, J., Liu, H., *et al.*: 'Application of the distributed generation, micro and smart power grid in the urban planning'. 4th Annual IEEE Int. Conf. Cyber Technol. Automation, Control and Intelligent Systems, Hong Kong, China, 2014, pp. 634–637

[2] Miret, J., Castilla, M., Camacho, A., *et al.*: 'Control scheme for photovoltaic three-phase inverters to minimize peak currents during unbalanced grid-voltage sags', *IEEE Trans. Power Electron.*, 2012, **27**, (10), pp. 4262–4271

[3] Malaye, D., Dange, K., Barhate, T., *et al.*: 'Current trends of implementing smart grid for enhancing the reliability of power utility network'. 2nd Int. Conf. on Communication Systems, Computing and IT Applications (CSCITA), Mumbai, India, 2017, pp. 281–285

[4] Babaei, S., Fardanesh, B., Bhattachanya, S.: 'High-power VSC-based simultaneous positive- and negative-sequence voltage regulator', *IEEE Trans. Power Delivery*, 2014, **29**, (5), pp. 2124–2135

[5] Sosa, J., Castilla, M., Miret, J., *et al.*: 'Control strategy to maximize the power capability of pv three-phase inverters during voltage sags', *IEEE Trans. Power Electron.*, 2016, **31**, (4), pp. 3314–3323

[6] Roldán-Pérez, J., García-Cerrada, A., Zamora-Macho, J., *et al.*: 'Helping all generations of photo-voltaic inverters ride-through voltage sags', *IET Power Electronics*, 2014, **7**, (10), pp. 2555–2563

[7] P.O.12.2: 'Technical requirements of wind power and photovoltaic facilities', (draft), Red Electrica, Madrid, Spain, 2008

[8] Valouch, V., Bejvl, M., Šimek, P., *et al.*: 'Power control of grid-connected converters under unbalanced voltage conditions', *IEEE Trans. Ind. Electron.*, 2015, **62**, (7), pp. 4241–4248

[9] Zhang, P., Zhang, G., Wang, H.: 'Control strategy of low voltage ride-through for grid-connected photovoltaic inverter'. IEEE 6th Int. Symp. on Power Electronics for Distributed Generation Systems (PEDG), Aachen, Germany, 2015, pp. 1–6

[10] Mirhosseini, M., Pou, J., Karanayil, B., *et al.*: 'Positive- and negative-sequence control of grid- connected photovoltaic systems under unbalanced voltage conditions'. Australasian Universities Power Engineering Conf. (AUPEC), Hobart, TAS, Australia, 2013, pp. 1–6

[11] Wang, F., Duarte, J., Hendrix, M.: 'Pliant active and reactive power control for grid-interactive converters under unbalanced voltage dips', *IEEE Trans. Power Electron.*, 2011, **26**, (5), pp. 1511–1521

[12] Li, K., Liu, J., Wang, Z., *et al.*: 'Strategies and operating point optimization of statcom control for voltage unbalance mitigation in three-phase three-wire systems', *IEEE Trans. Power Deliv.*, 2007, **22**, (1), pp. 413–422

[13] Rodriguez, P., Medeiros, G., Luna, A., *et al.*: 'Safe current injection strategies for a statcom under asymmetrical grid faults'. IEEE Energy Conversion Congress and Exposition, Atlanta, GA, USA, 2010, pp. 3929–3935

[14] Teodorescu, R., Liserre, M., Rodriguez, P.: '*Grid converters for photovoltaic and wind power systems*' (John Willey & Sons, Chichester, 2011, 1st Edn.)

[15] Khoshooei, A., Moghani, J., Candela, I., *et al.*: 'Control of DSTATCOM during unbalanced grid faults based on DC voltage oscillations and peak', *IEEE Trans. Ind. Appl.*, 2018, **54**, (2), pp. 1680–1690

[16] García-Gracia, M., El Halabi, N., Ajami, H., *et al.*: 'Integrated control technique for compliance of solar photovoltaic installation grid codes', *IEEE Trans. Energy Convers.*, 2012, **27**, (3), pp. 792–798

[17] Sadeghkhani, I., Hamedani-Golshan, M. E., Guerrero, J.M., *et al.*: 'A current limiting strategy to improve fault ride-through of inverter interfaced autonomous microgrids', *IEEE Trans Smart Grid*, 2017, **8**, (5), pp. 2138–2148

[18] Bottrell, N., Green, T.C.: 'Comparison of current-limiting strategies during fault ride-through of inverters to prevent latch-up and wind-up', *IEEE Trans. Power Electron.*, 2014, **29**, (7), pp. 3786–3797

[19] Baghaee, H.R., Mirsalim, M., Gharehpetian, G.B., *et al.*: 'A new current limiting strategy and fault model to improve fault ride-through capability of inverter interfaced DERs in autonomous microgrids', *Sust. Energy Technol. Assess.*, 2017, **24**, pp. 71–81

[20] Baghaee, H.R., Mirsalim, M., Gharehpetian, G.B., *et al.*: 'OC/OL protection of droop-controlled and directly voltage-controlled microgrids using TMF/ANN-based fault detection and discrimination', *IEEE J Emerging Sel Topics Power Electron*, 2019, DOI 10.1109/JESTPE.2019.2958925, in press

[21] Mahamedi, B., Eskandari, M., Fletcher, J.E., *et al.*: 'Sequence-based control strategy with current limiting for the fault ride-through of inverter-interfaced distributed generators', *IEEE Trans. Sust. Energy*, 2020, **11**, (1), pp. 165–174

[22] Guo, X., Liu, W., Lu, Z.: 'Flexible power regulation and current-limited control of the grid-connected inverter under unbalanced grid voltage faults', *IEEE Trans. Ind. Electron.*, 2017, **64**, (9), pp. 7425–7432

[23] Chen, H., Lee, C., Cheng, P., *et al.*: 'A low-voltage ride-through technique for grid-connected converters with reduced power transistors stress', *IEEE Trans. Power Electron.*, 2016, **31**, (12), pp. 8562–8571

[24] Tafti, H.D., Maswood, A.I., Konstantinou, G., *et al.*: 'Active/reactive power control of photovoltaic grid-tied inverters with peak current limitation and zero active power oscillation during unbalanced voltage sags', *IET Power Electron*, 2018, **11**, (6), pp. 1066–1073

[25] Camacho, A., Castilla, M., Miret, J., *et al.*: 'Active and reactive power strategies with peak current limitation for distributed generation inverters during unbalanced grid faults', *IEEE Trans. Ind. Electron.*, 2015, **62**, (3), pp. 1515–1525

[26] Lopez, M., García de Vicuña, L., Miret, J., *et al.*: 'Control strategy for grid-connected three-phase inverters during voltage sags to meet grid codes and to maximize power delivery capability', *IEEE Trans. Power Electron.*, 2018, **33**, (11), pp. 9360–9374

[27] Afshari, E., Moradi, G., Rahimi, R., *et al.*: 'Control strategy for three-phase grid-connected PV inverters enabling current limitation under unbalanced faults', *IEEE Trans. Ind. Electron.*, 2017, **64**, (11), pp. 8908–8918

[28] Camacho, A., Castilla, M., Miret, J., *et al.*: 'Positive and negative sequence control strategies to maximize the voltage support in resistive – inductive grids during grid faults', *IEEE Trans. Power Electron.*, 2018, **33**, (6), pp. 5362–5373

[29] Rolán, A., Giménez, P., Yagüe, S., *et al.*: 'Voltage recovery influence on three-phase grid-connected inverters under voltage sags', *IET Gener. Transm. Distrib.*, 2019, **13**, (3), pp. 435–443

[30] Spanish Ministry of Industry, Tourism and Commercial BOE-A-2005-3419. 'Resolution of February 11th, 2005, from General Secretary of Energy, by which it is approved a set of technical and Instrumental Procedures Needed to do an Adequate Technical Management of the Electrical System', 2005

[31] Bollen, M., Yu-Hua Gu, I.: '*Signal processing of power quality disturbances*' (Wiley-IEEE Press, New York, NY, USA, 2005, 1st Edn.)

[32] Bollen, M.: '*Understanding power quality problems voltage sags and interruptions*' (Wiley-IEEE Press., New York, 2000, 1st Edn.)

[33] Guasch, L., Córcoles, F., Pedra, J.: 'Effects of symmetrical and unsymmetrical voltage sags on induction machines', *IEEE Trans. Power Delivery*, 2004, **19**, (2), pp. 774–782

[34] Ku, Y.H.: 'Transient analysis of ac machinery', *AIEE Trans.*, 1929, **48**, (3), pp. 707–714

[35] Fortescue, C.: 'Method of symmetrical co-ordinates applied to the solution of polyphase networks'. *Trans. Am. Inst. Electr. Eng.*, 1918, **37**, (2), pp. 1027–1140

[36] Sarkar, M.N.I., Meegahapola, L.G., Datta, M.: 'Reactive power management in renewable rich power grids: A review of grid-codes, renewable generators, support devices, control strategies and optimization algorithms', *IEEE. Access.*, 2018, **6**, pp. 41458–41489

[37] Akagi, H., Watanabe, E.-H., Aredes, M.: '*Instantaneous power theory and applications to power conditioning*' (IEEE Press., Hoboken, 2017, 2nd Edn.)

[38] Bakkar, M., Bogarra, S., Córcoles, F., *et al.*: 'Power control strategies during voltage sags according to spanish grid code'. Int. Conf. on Renewable Energies and Power Quality, Spain, 2018, pp. 493–498